Science of the Total Environment 896 (2023) 165293

Contents lists available at ScienceDirect

Science of the Total Environment

journal homepage: www.elsevier.com/locate/scitotenv

The genesis of an extremely acidic perched aquifer within roasted pyrite waste in a fully urbanized area (Zaragoza, Spain)

Jon Jiménez Beltrán [a,b], Miguel Ángel Marazuela [a], Carlos Baquedano [a], Jorge Martínez-León [a], Jose Ángel Sanchez Navarro [b], Noelia Cruz-Pérez [c], Juan C. Santamarta [c], Alejandro García-Gil [a,*]

[a] Geological and Mining Institute of Spain (IGME-CSIC), Spanish National Research Council, C/Ríos Rosas 23, 28003 Madrid. Spain
[b] Department of Earth Sciences, University of Zaragoza, c/ Pedro Cerbuna 12, 50009 Zaragoza, Spain
[c] Departamento de Ingeniería Agraria y del Medio Natural, Universidad de La Laguna (ULL), La Laguna (Tenerife), C/ Pedro Herrera, s/n, 38200 San Cristóbal de La Laguna, Spain

HIGHLIGHTS

- Water stagnation due to concrete barriers enhances acid drainage problems in urban areas.
- Acid drainage from pyrite oxidation leading to SO_4-rich waters increases concrete dissolution.
- Water residence time may control acid drainage development in urban areas.
- An extreme acidity (pH < 2) front propagates due to differential residence times.
- Water collectors and restriction of recharge can prevent acid drainage in urban areas.

GRAPHICAL ABSTRACT

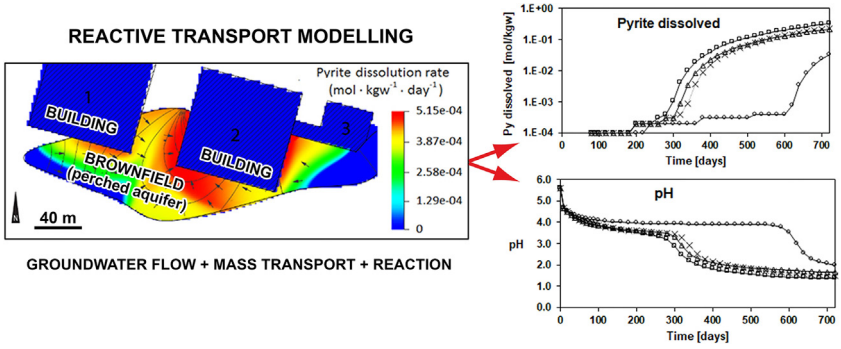

ARTICLE INFO

Editor: Damia Barcelo

Keywords:
Contamination
Urban aquifer
Perched aquifer, reactive transport
Acid drainage
Sulphide oxidation

ABSTRACT

Contaminated groundwater is a serious problem in developed countries. The abandonment of industrial waste may lead to acid drainage affecting groundwater and severely impacting the environment and urban infrastructure. We examined the hydrogeology and hydrochemistry of an urban area in Almozara (Zaragoza, Spain); built over an old industrial zone, with pyrite roasting waste deposits, there were acid drainage problems in underground car parks. Drilling and piezometer construction, and groundwater samples revealed the existence of a perched aquifer within old sulfide mill tailings, where the building basements interrupted groundwater flow, leading to a water stagnation zone that reached extreme acidity values (pH < 2). A groundwater flow reactive transport model was developed using PHAST to reproduce flow and groundwater chemistry, in order to be used as a predictive tool for guiding remediation actions. The model reproduced the measured groundwater chemistry by simulating the kinetically controlled pyrite and portlandite dissolution. The model predicts that an extreme acidity front (pH < 2), coincident with the Fe (III) pyrite oxidation mechanism taking dominance, is propagating by 30 m/year if constant flow is assumed. The incomplete dissolution of residual pyrite (up to 18 % dissolved) predicted by the model indicates that the acid drainage is limited by the flow regime rather than sulfide availability. The installation of additional water collectors between the recharge source and the stagnation zone has been proposed, together with periodic pumping of the stagnation zone. The study findings are expected to serve as a useful background for the assessment of acid drainage in urban areas, since urbanization of old industrial land is rapidly increasing worldwide.

* Corresponding author.
E-mail address: a.garcia@igme.es (A. García-Gil).

http://dx.doi.org/10.1016/j.scitotenv.2023.165293
Received 30 March 2023; Received in revised form 1 July 2023; Accepted 1 July 2023
Available online 4 July 2023

1. Introduction

Demand for land is rapidly increasing as the population in Europe grows (Eurostat., 2016). Urban sprawl tends to create rapid urbanization of industrial sites (Chen et al., 2018; Chen and Ye, 2014; Jarah et al., 2019). Sustainable urban development requires revitalizing and remediating contaminated land that is a legacy of past industrial sites. Industrial complexes in urban areas may enhance the environmental hazard due to unregulated or insufficient waste management policies (Allen et al., 1999). This industrial heritage in Europe and poor environmental management policies have left a legacy of contaminated sites, which pose a risk to human health and the environment (Ana, 2018). Urbanization of these industrialized areas, known as *brownfields* (Meuser, 2010), may lead to shorter life expectancy, lower quality of life (Bech, 2020) and psychosocial issues (Bambra et al., 2014).

Soils in brownfields may contain large amounts of mineral pollutants that have accumulated over time, thus producing high pollution concentrations or loadings of As, Ba, Cd, Co, Cr, Cu, Hg, Pb, Mo, Ni, V, and Zn (Li et al., 2013; Wong et al., 2006). In particular, brownfields from mining and the metallurgical and processing industries are especially contaminated by a large number of heavy metals, which eventually contaminate groundwater (Del Giudice et al., 2020; Solcova et al., 2022). The environmental problems, including air, land, and water pollution, arise from abandoned tailings, tailings piles, or disposal ponds and have been a topic of concern for many years (Hossner and Hons, 1992; Kefeni et al., 2017). Abandoned tailings often contain sulfide-bearing minerals (pyrite, pyrrhotite, chalcopyrite, arsenopyrite, cobaltite), with high potential for generating acid drainage (Berg et al., 1975; Fuller and Lanspa, 1975; Sorensen et al., 1980). Oxidation of ferrous iron by oxygen in abandoned tailings (Eq. (1)) is considered much slower than the oxidation of iron disulfide by ferric iron (Eq. (2)). Once pH is reduced down to approximately 3, the reaction from Eq. (2) is catalyzed by the *Thiobaccillus ferroxidans* iron oxidizing bacteria (Nordstrom, 2000).

$$2FeS_2 + 15/2\ O_2 + 7H_2O = 2Fe(OH)_3 + 4H_2SO_4 \quad (1)$$

$$FeS_2 + 14Fe^{3+} + O_2 + 8H_2O = 15Fe^{2+} + 2SO_4{}^{2} - + 16H^{+} \quad (2)$$

These reactions lead to extremely low pH values in the abandoned tailings environment, resulting in increased solubility of the constituent minerals and in the mobilization of the mentioned heavy metals. In such environments, pH measurements of tailings drainage ranging from 2.9 to 4.2 and maximum concentrations of sulfate 4.200 $mg{\cdot}L^{-1}$, Fe 1.860 $mg{\cdot}L^{-1}$, and Mn 286 $mg{\cdot}L^{-1}$ are typically found (Dean, 1982).

Acidification of water by mining waste and the potential environmental impacts on soils and water resources is a widely studied and documented topic (e.g., Bell et al., 1989; Egiebor and Oni, 2007; Elliott et al., 1998; Kefeni et al., 2017; Nordstrom, 2000; Song et al., 2022). In addition to the extremely low pH in affected waters, the severe impacts of acid drainage are related to the subsequent mobilization and spread of toxic heavy metals such as As, Fe, Cu, Cd, Ni, Pb, and Zn in highly oxidizing environments, and to the high SO_4^{2-} concentrations reached (Tomiyama and Igarashi, 2022). Once the acid drainage has spread through the soils and waters, there are high treatment costs to controlling and remediating the pollution processes (Anawar, 2015; Chen et al., 2021), with estimated remediation costs up to 500M USD/year for abandoned mining waste deposits (Naidu et al., 2019). However, the recovery of rare earth elements from acid drainage can potentially offset the costs of acid drainage treatment (Ayora et al., 2016). Different remediation processes are widely used to mitigate the acid drainage effects, including chemical neutralization, adsorption, wetland construction, microorganisms and membrane technologies (Chen et al., 2021). The risk assessment before using these methods requires highly precise site characterization and quantification of the acid drainage spread. During the last decades, the development of numerical models with the capability to simulate multicomponent reactions and transport in 3D heterogeneous media has provided a precise tool for risk assessment and remediation of acid drainage (Malmström et al., 2008). However, the development of acid mine drainage in a fully urbanized area is infrequent and these areas include additional heterogeneities with respect to the natural environments, such as different minerals from concrete used in the buildings (e.g., portlandite) and artificial physical barriers that can drastically control the flow regime. In Spain, there are some important examples, namely Huelva, in which urban acid drainage related to mining activities in the Pyrite Belt was investigated (Guillén et al., 2011). This acid drainage was spread through the Tinto and Odiel rivers, which drain the world's largest sulfide mineral formation (the Iberian Pyrite Belt) to their estuarine zones, where increased concentrations of Ni, Cd and As were measured. These elements were not prone to be removed out of solution due to precipitation/adsorption, unlike Fe, Al, Co, Cu, Mn, Pb, Zn, and Th (Hierro et al., 2014). There are limited reports of acid drainage occurrence in urban areas worldwide, the drinking groundwaters from the urban area of Perth (Western Australia), for instance, which have been enriched in As (7000 μg/L) due to the exposure of pyritic sediments (Appleyard et al., 2006).

Sulfide-bearing minerals are also commonly found in brownfields containing waste generated from the production of sulfuric acid for the fertilizer industry. Residue from the roasting of pyrite ore to obtain sulfuric acid used in the fertilizer industry extends worldwide (Runkel and Sturm, 2009). The roasting process produces a residue known as pyrite ash, composed mainly of iron-oxides (hematite) and secondary minerals (anglesite), and high concentrations of Pb, Zn and Cu (Gabarrón et al., 2018; Oliveira et al., 2012). The environmental impacts of residual pyrite ash have been widely documented to be acid drainage, water erosion and runoff, loss of vegetation and spreading of particles containing metals by wind erosion (Kong et al., 2011). During the mid-20th century in Spain, the production of sulfuric acid by pyrite roasting was a common industrial activity. Unfortunately, the mismanagement of pyrite ash in Spain led to serious environmental problems (Domènech et al., 2017). A notable example is found in the industry legacy of Cartagena (southeast Spain), where pyrite ash waste was landfilled over a number of ponds (Soriano-Disla et al., 2018). Environmental risk management of affected areas still represents a major challenge worldwide (Hiji et al., 2014; Lin and Quvarfort, 1996; Pérez-López et al., 2007; Soriano-Disla et al., 2018; Vasilache et al., 2022).

In this study, the acid drainage generated in an industrial brownfield with buried pyrite ash waste, located in the area of Almozara (Zaragoza), was characterized and modelled. This acid drainage generated an extremely acidic perched aquifer. This paper aims to explain the hydrogeological conditions and the geochemical reactions that led to the genesis of this acidic perched aquifer and provides an example of redevelopment of post-industrial districts in the city of Zaragoza (Spain). The main research questions addressed in this article are as follows: 1) Assessing the influence of urban environmental elements such as physical barriers formed by building foundations or retaining walls constructed as a mitigation measure for acid drainage on the geochemical evolution of the aquifer 2) Identifying the key parameters and limiting factors controlling the oxidation and dissolution of sulfides that lead to rapid acidification of the perched aquifer 3) Considering the aforementioned limiting factors, determining the most suitable acid drainage mitigation procedures for Almozara in the future. For this purpose, the hydrogeological and hydrochemical characterization of the perched aquifer is described; the genesis of the acid drainage generation is examined and reproduced numerically by means of a reactive transport model of the perched aquifer. Finally, considering the outcomes of the reactive transport model, the results of the successful remediation actions taken and most efficient future management procedures are discussed.

2. Study area

2.1. Historical industrial legacy: pyrite ash tailings

The investigated site corresponds to an alluvial aquifer (Fig. 1) located in the urban area of Zaragoza (Spain). In 1899, an industrial complex

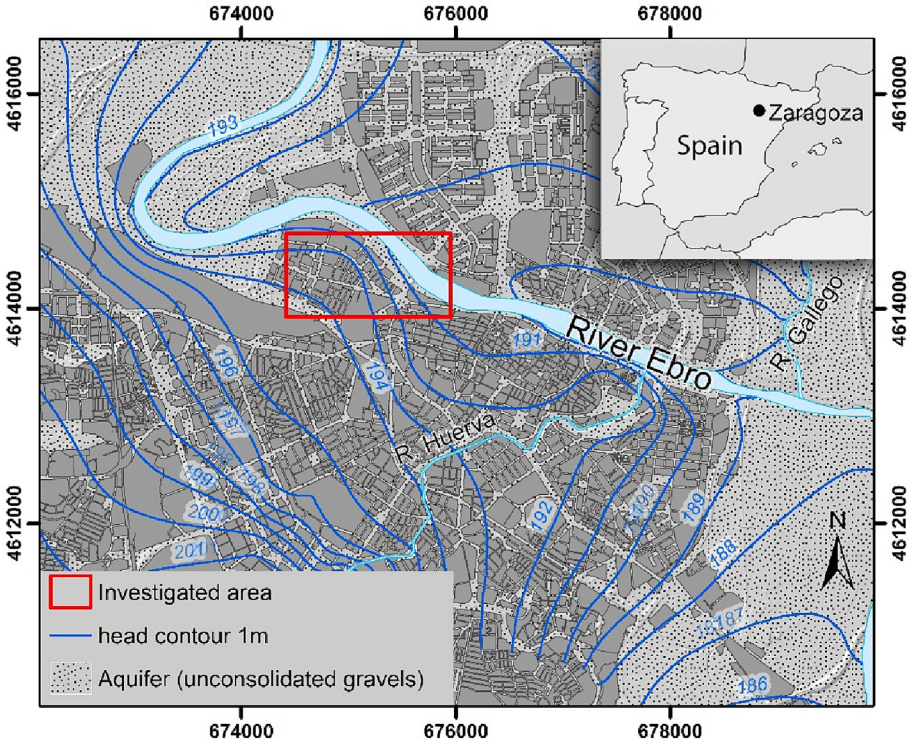

Fig. 1. Location of the investigated area. Projection: WGS 1984 Complex UTM Zone 30 N, Datum DWGS1984.

dedicated to the production of fertilizers called *La Industrial Química de Zaragoza* (Fig. 2) was established in the study area. In order to produce sulfuric sulfuric sulfuric sulfuric acid, sulfide ore roasting was included in the industrial complex activities. This process resulted in the accumulation of a large amount of sulfide (mainly pyrite) and associated pyrite ash. Specifically, the cumulative industrial waste consisted primarily of sulfides, mainly pyrite (FeS_2), sphalerite (ZnS), chalcopyrite ($CuFeS_2$) and arsenopyrite (FeAsS), and iron slag (TPA, 2001). The industrial complex occupied 85,000 m^2 of the Ebro's fluvial terraces, located at about 360 m from the Ebro River (Fig. 1). In the 1960s, the city's growth around the complex led to an uncomfortable and unhealthy situation. In 1977, the municipal authority identified the industrial complex as a contamination source and forced the company to end industrial activity in that location. The industrial complex move was financed with the land sale, and >2000 apartments and a public park (see the aerial photography from 2006 in Fig. 2) were built directly on top of the rubble and mixed waste, containing pyrite ash.

Extremely acidic leakage (pH < 2) was observed in some building foundations (red arrow in Fig. 2) in 2001 (TPA, 2001). In response to evident environmental problems related to old industrial waste on the land parcel, the Zaragoza City Council constructed a rainwater trap system, which consisted of a drainage ditch, for the mitigation of the risks associated with metals in pyrite ash. To design and construct the drainage system, as well as monitoring and surveilling the recovery of the polluted perched aquifer, the City Council commissioned a piezometer network, which allowed identification of a perched aquifer developed in old pyrite ash tailings (TPA, 2001). In 2005, the rainwater collector system was built, three years before starting the research, tests and associated results presented in this work.

2.2. Hydrogeological settings

The investigated aquifer consists of typical alluvial deposits and floodplain terraces, configuring an unconfined aquifer hydraulically connected with the Ebro River (García-Gil et al., 2020; Garcia-Gil et al., 2014; García-Gil et al., 2015). The water table in the studied area is in the range of 7 to 8 m depth, and the main groundwater flow is SW-NE. The contaminated perched water body, located 1 to 4 m deep (TPA, 2001), is clearly differentiated from the 7 m deep water table of the Ebro river aquifer (Garcia-Gil et al., 2014). The 33 piezometer network (Fig. 3) commissioned by the Zaragoza City Council showed the extent of the perched aquifer, exceeding 25,000 m^2 (Alcaraz et al., 2016). During the drilling of the piezometers, a layer of rubble industrial waste containing pyrite ash was identified at 30 to 50 cm under the surface. This layer presented a variable thickness, ranging from 1 to 3 m.

The main hydrochemical characteristics of the groundwater samples taken from the perched aquifer in 2001 (TPA, 2001) (before the water collector was installed in 2005) are summarized in Table 1, which shows minimum pH values below 2, and extremely high concentrations of Fe, Cu and Zn, reaching values of grams per liter. In 2001, the presence of extremely acidic water was found in piezometers S-2, S-3, S-27, S-28, S-29, S-30 and S-31, all of them located between buildings 2 and 3 (Fig. 3), which is the stagnation zone of the perched aquifer. Measured pH values ranged from 1.5 to 2 and conductivity ranged from 9000 to 15,000 $\mu S \cdot cm^{-1}$ (approximately 10 times as high as the alluvial water with which the perched aquifer is recharged). Sulfate content (up to 57 g/L) dominates among the major ions detected, and a very low sodium content (<5 mg/L) was found. However, the most remarkable feature was the high content of heavy metals which, in the case of Cu, Zn and Fe, was up to grams per liter in order of magnitude. All previous concentrations will be compared to the measurements obtained from the same piezometers during the 2008 campaign conducted for this study, in order to assess the effect of installation of the water collector on the evolution of acid drainage in the perched aquifer. Additionally, a reactive transport model will be used to reconstruct the concentrations measured in 2001 (when the acid drainage had its maximum incidence), in order to better understand and quantify the primary reactions and limiting factors influencing the observed geochemical evolution of the acid drainage.

In a 3000 m^2 area located between buildings 2 and 3, shown in Fig. 3, an especially problematic area was identified, which coincides with the acidic water leaks found inside building basements. In this area, prior to the construction of the rainwater trap that runs through it, three pumping tests were conducted (S-2, S-27 and S-29 piezometers), obtaining an average permeability for the industrial waste of 1.5 $m \cdot day^{-1}$. The volume of contaminated water was estimated to range from 300 to 400 m^3.

Fig. 2. Aerial photography of the industrial complex in 1956, 1986 and 2005. Location of acid leakage area is marked by a red polygon.

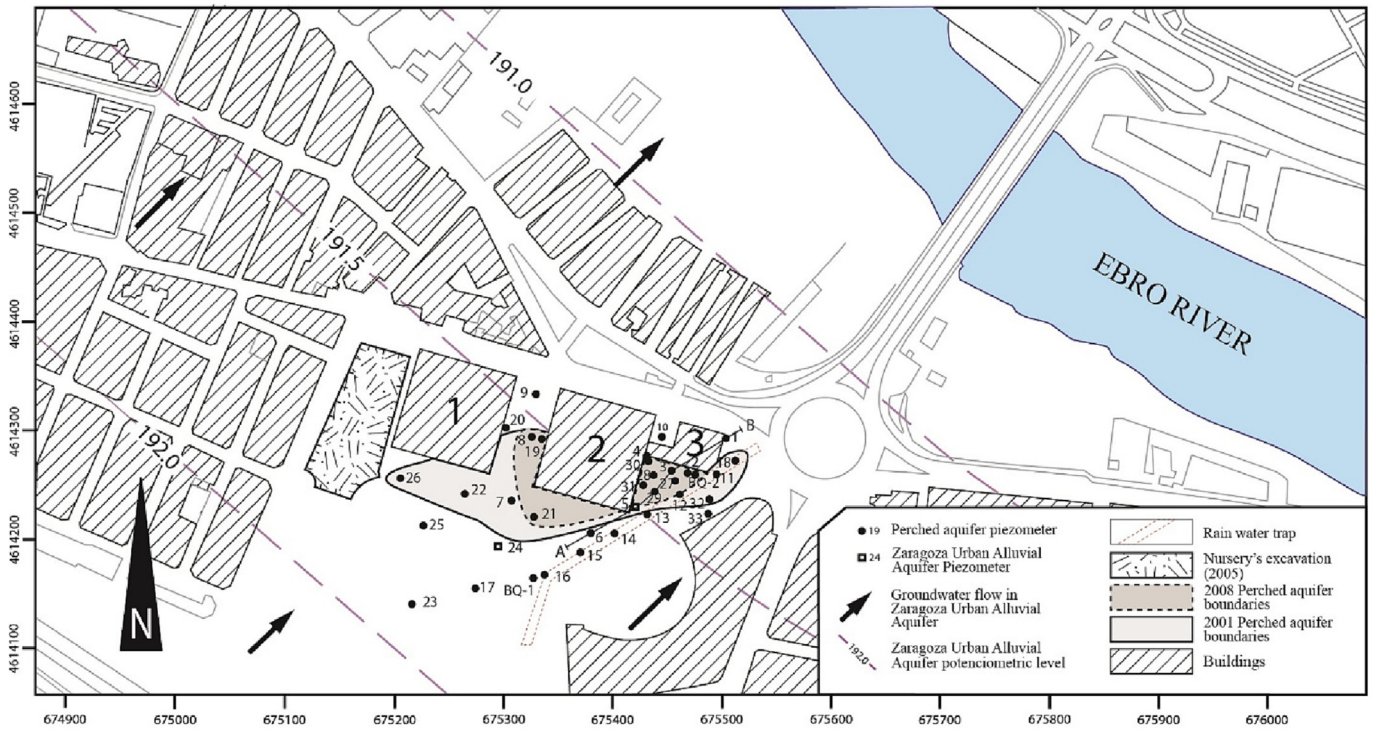

Fig. 3. Location of the piezometer monitoring network. Perched aquifer boundaries by TPA (2001) Projection: WGS 1984 Complex UTM Zone 30 N, Datum DWGS1984.

Table 1
First analytical results from groundwater (GW) samples obtained from the piezometer monitoring network in 2001 (TPA, 2001).

Piezometer	GW depth	pH	EC	SO_4^{2-}	PO_4^{3-}	Cl^-	Pb	Zn	Cu	As	Fe	Cd	Cr
	[m]	[−]	[μS·cm^{-1}]	[mg·L^{-1}]	[mg·L^{-1}]	[mg·L^{-1}]	[mg·L^{-1}]	[mg·L^{-1}]	[mg·L^{-1}]	[mg·L^{-1}]	[mg·L^{-1}]	[mg·L^{-1}]	[mg·L^{-1}]
S-11	2.2	2.5	9230	10,357	0.6	426	<0.1	920.00	500.0	0.048	455.0	2.75	<0.2
S-12	2.0	2.0	19,540	17,952	4.0	958	<0.1	850.00	1290.0	0.124	1260.0	9.00	0.5
S-18	2.2	2.2	4120	4106	<0.1	284	<0.1	81.20	55.0	0.027	38.0	0.98	<0.2
S-19	4.0	5.0	4890	2857	<0.1	639	<0.1	14.25	18.0	<0.001	0.4	0.98	<0.2
S-21	3.6	5.3	5580	1850	<0.1	692	<0.1	0.57	0.2	0.060	5.6	<0.02	<0.2
S-22	3.3	6.1	4880	2976	3.7	674	0.1	3.79	1.4	0.143	46.2	0.03	<0.2
S-26	2.1	6.0	3920	3214	20.5	639	<0.1	0.05	0.2	0.061	0.9	<0.02	<0.2
S-27	1.9	1.9	18,240	17,714	2.1	852	0.3	2120.00	1550.0	0.282	1700.0	13.00	0.6
S-28	2.0	1.9	19,110	13,571	13.1	887	0.1	3570.00	1100.0	2.900	6400.0	9.00	0.8
S-29	1.8	2.0	16,040	12,380	13.3	1242	0.3	2860.00	760.0	1.300	7250.0	7.00	0.6
S-30	2.0	2.4	18,850	12,857	11.4	1065	<0.1	6660.00	2080.0	4.000	3210.0	16.00	1.0
S-31	1.7	2.0	20,200	14,047	23.5	1065	0.2	5920.00	1750.0	5.600	5950.0	12.00	1.0
S-32	4.7	3.0	7150	4523	<0.1	532	<0.1	7.00	130.0	<0.001	7.0	2.48	<0.2

3. Materials and methods

3.1. Sampling campaign

During the month of March 2008, a hydrogeological campaign was carried out to evaluate groundwater levels, measure in-situ physico-chemical parameters and obtain groundwater samples from the perched aquifer. From each piezometer of the monitoring network, built in 2001 (Fig. 3), the values of electrical conductivity (as μS·cm^{-1} at 20 °C), temperature, and pH were measured in-situ. Additionally, groundwater samples were taken from each piezometer for the determination of major cations (Ca^{2+}, Mg^{2+}, Na^+ and K^+), anions (SO_4^{2-}), and several metal concentrations of interest related to pyrite ash contamination (Cu, Fe and Zn). A total of 11 samples were collected where contaminated water still remained, and they were analysed in accredited laboratories according to 872/LE1620 Spanish National Accreditation Body (ENAC). Groundwater samples were collected from the piezometers at the upper section of the water column. Conductivity measurements were obtained in situ using a conductivity meter with automated temperature correction. The samples were carefully transferred into sterilized polypropylene bottles and kept refrigerated and protected from light until they were delivered to the laboratory.

3.2. Reactive transport model

In order to reproduce the hydrochemical properties of the acid perched aquifer, hosted in the pyrite ash waste from an initial solution of irrigation water recharge, a reactive transport model was implemented. The PHAST (Charlton and Parkhurst, 2011; Parkhurst et al., 2004) code developed by the U.S. Geological Survey was utilized. This code allows modeling of groundwater flow and associated solute transport with the capability to simulate chemical reactions. The chemical reaction module of the code is derived from PHREEQC (Parkhurst and Appelo, 2013). PHAST code was selected to reproduce, in a multidimensional dynamic system, the full range of equilibrium and kinetic geochemical reactions controlling the pyrite dissolution and the precipitation of several secondary minerals.

3.2.1. Flow and solute transport calculations

A 3-D flow model embedding a heterogeneous distribution of lithological materials was set up to simulate groundwater flow in the perched aquifer. The spatial discretization and boundary conditions of the selected domain are shown in Fig. 4. The possible effects of vertical flow on the reactive and transport calculations were considered negligible compared to horizontal flow, since the pyrite roasting waste deposits show reduced thickness compared to their lateral dimension (TPA, 2001). Thus, only one horizontal layer with discrete grid elements along the two horizontal dimensions was used in the numerical model. The resulting grid was 204 × 95 × 1 elements, covering a 350 × 120 m surface and a 2 m depth unique horizontal layer, which is the approximate average thickness of the pyrite roasting waste deposits in the area affected by acid drainage. The model assumed a steady-state flow regime under confined conditions, since there were no changes in groundwater levels conditioning its transmissivity. Two different porous media were discretized in the active domain – the perched aquifer and the buildings (Fig. 4). The imposed hydraulic regime corresponded to calibrated recharge which reproduced 2001 groundwater level measurements (TPA, 2001), adopting a hydraulic conductivity of 1.5 m·day^{-1}. The later value was obtained from a pumping test carried out in the perched aquifer (TPA, 2001). For the buildings, 10^{-7} m·day^{-1} hydraulic conductivity was adopted as a low permeability zone. A porosity of 0.2 and 10^{-4} were imposed to aquifer and building materials, respectively. Boundary conditions imposed for the groundwater flow problem were first-type for the cells in the three output points inferred from the head contour maps, and second-type for the prescribed constant flow of $2.82{\cdot}10^{-3}$ m^3·day^{-1}·m^{-2} as surface recharge from the existent parks in the domain (Fig. 4). Transient state was considered for the transport problem, running the simulation for two years with a time step of one day. To solve the transport problem, boundary conditions of first-type, with prescribed constant concentration, were imposed in the recharge and output zones. The initial solution imposed corresponded to a groundwater sample (pH = 7.3, Na = 141 mg/L, Cl = 236 mg/L, SO_4 = 299 mg/L, K = 2.7 mg/L, Ca = 200 mg/L, Mg = 38 mg/L, Fe = 0.1 mg/L; CHE, 2023) of the Ebro alluvial aquifer, since it is the water used for irrigation of the affected area.

3.2.2. Reactive transport calculations

To solve the reactive transport problem, the chemical reactions modelled were kinetically controlled pyrite oxidation, using the rates for oxidation mechanisms by O_2 and Fe^{3+} compiled by Williamson and Rimstidt (1994), and thermodynamically controlled precipitation, imposing a constant value of SI = 0 in case oversaturation was reached, of two of the most common secondary minerals in the acid drainage of pyrite tailings: ferrihydrite and jarosite-K (Huminicki and Rimstidt, 2009). Many other secondary minerals have been documented to precipitate in similar geochemical conditions, such as melanterite, ettringite, etc. (Grundl and Delwiche, 1993). However, after calculating the evolution of the saturation index of these secondary minerals during pyrite oxidation, using PHREEQC, only ferrihydrite and jarosite-K were prone to precipitate, so only these phases were allowed to precipitate as secondary minerals in the reactive transport model.

The analysis of pyrite ash performed by López Julián et al., 2020 was adopted to estimate the initial available amount of pyrite residuals (mol/kg of water) in the pyrite ash and the possible secondary minerals precipitated. In that analysis, the presence of <5 % of pyrite and the secondary mineral jarosite were reported. A more precise estimated value of the volumetric fraction of residual pyrite can be found in the work by Lin and Quvarfort (1996), which reported a 2 % mass of residual pyrite, consistent

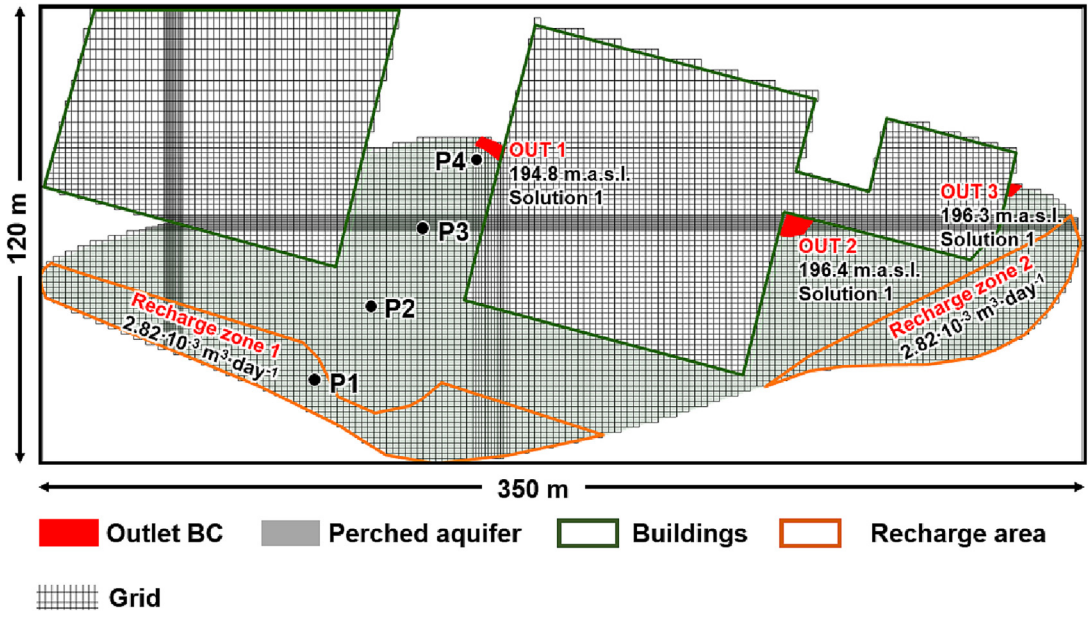

Fig. 4. Model domain discretization, and flow and transport boundary conditions.

with the range of <5 % estimated for the Almozara pyrite ash deposit. Thus, a 2 % initial mass of pyrite for the reactive transport model was set to obtain the initial molality of 1.6 mol/kg. Next, to calculate the reactive surface of pyrite in the aquifer (in m^2/kg of water), the approximation method of cubical grains of dimension *d* from Lichtner (1996) was applied, usingthe equation:

$$s = \frac{6}{d}\cdot(1-\varphi) = \frac{6}{0.002}\cdot(1-0.2) = 2400\ \ m^2\cdot m^{-3} \quad (3)$$

where *s* is the specific surface area of the grains in m^2/m^3, *d* is the grain size in m (with an average of 2 mm, as reported by López Julián et al., 2020), and φ is the porosity of the pyrite ash. Finally, considering the previous mass fraction of 2 % for pyrite and the calculated specific surface area of the pyrite grains, the reactive surface area of the pyrite in the aquifer was estimated to be 0.192 m^2/kg of water, thus setting this value in the reactive transport model. In line with this approximation, it is noteworthy to highlight that the heterogeneity of the aquifer materials constituted by a mixture of pyrite roasting waste and concrete from old building debris represents one of the main limitations of the numerical model. In particular, the uncertainty linked to heterogeneous porosity, particle size and mineral proportions (e.g., particle size distribution of residual sulfides) along the perched aquifer may significantly affect both the water/rock volume ratio and the reactive surface of the minerals considered. Nevertheless, given the known evolution of the chemical composition of the perched aquifer, the similarity between the measured final chemical compositions and the final computed concentrations can be used in this case as validation criterion.

Finally, in the polygons that correspond to the concrete walls of the building basements, an additional reaction of kinetically controlled portlandite dissolution was considered to assess the possible effect of pH neutralization and Ca release on the other reactions modelled. In this case, there was no available information regarding the portlandite reactive surface, volumetric fraction or precise dissolution rates in literature or in the samples. However, given that concrete is the only material controlling Ca release in this aquifer, and that the final Ca concentrations measured in the samples could also be used, the portlandite dissolution rate was calibrated to obtain the measured Ca concentrations in the order of magnitude as the best possible estimation for this model. This estimation will be considered in the discussion of the model limitations.

4. Results and discussion

4.1. Acid drainage characterization by direct observations in piezometers and groundwater chemical analyses

The observations and tests carried out in the piezometers placed in the affected area, as well as the groundwater sample analyses performed in 2001 and 2008(before and after the rainwater trap was constructed), enabled a comparison of the effect of this structure on the extension, depth and hydrochemical parameters of the perched aquifer. Table 2 shows the water levels measured in the piezometers in March 2008, confirming the persistence of the perched aquifer, but to a reduced extent compared to 2001. Recharge comes mainly from irrigation of the gardens. This irrigation water is pumped by City Council wells from the regional alluvial aquifer of the Ebro River. The alluvial aquifer water showed a calcium - sulfate composition, a neutral pH of 7.3 and a conductivity of 1305 μS·cm^{-1} (CHE, 2023). Fig. 5 compares 2001 and 2008 aquifer water levels, highlighting the impact of the rainwater trap constructed in 2005. This collector system reduced the extent of the perched aquifer. In fact, the perched aquifer has disappeared in seven piezometers. However, in the area between buildings 2 and 3, which is the most problematic area, the perched aquifer remains, with a water table about 2.6 m deep, slightly below the water table measured in 2001, which was around 2.1 m deep.

Fig. 6 shows a hydrogeological cross-section of the perched aquifer and its relation to the surrounding buildings. The head contour map shown in Fig. 5 suggests that the perched aquifer recharge occurs mainly by direct infiltration from the green areas on the surface. Since the construction of the public park, its irrigation system provides an equivalent precipitation to the aquifer of >1000 mm every six months, whereas the average annual rainfall of the area is 350 mm. At the same time, aquifer recharge can occur thanks to irrigation network losses. With the partial lawn substitution of xeriscapes, the recharge has decreased significantly. In addition, if the rainwater collector is considered, the reason for the reduction of the perched aquifer is found to be consistent with the effect of this remediation structure (Fig. 5B). The remaining groundwater is below the collector's topographic height. However, the effect of acid drainage on the building basements still represents a main concern, despite the water collector reducing the extent of the perched aquifer, and this effectwill be quantified by the numerical model implemented in order to discuss future management possibilities.

Table 2
Groundwater levels measurement and hydrochemical analysis results from the piezometer network of the investigated perched aquifer in 2008.

Piezometer-sample	GW depth [m]	Cond. [$\mu S \cdot cm^{-1}$]	Ca [$mg \cdot L^{-1}$]	Mg [$mg \cdot L^{-1}$]	Na [$mg \cdot L^{-1}$]	K [$mg \cdot L^{-1}$]	SO_4^{2-} [$mg \cdot L^{-1}$]	Cu [$mg \cdot L^{-1}$]	Zn [$mg \cdot L^{-1}$]	Fe [$mg \cdot L^{-1}$]
S-2	2.60	9061	444.8	125.9	<5	<5	19,554	1100.0	206.7	844.6
S-3	2.65	9554	338.9	147.1	1.2	<5	13,604	108.10	258.3	928.8
S-4	2.75	3024	838.0	18.0.	40.6	62	2504	<0.50	0.7	<0.1
S-8	2.80	5752	575.8	97.5	117.8	440.2	3318	9.00	67.4	0.67
S-10	2.70	5325	684.0	397.9	188.8	67.6	5041	0.09	0.7	0.36
S-19	3.84	4283	552.4	109.5	71.0	141.2	3223	1.17	6.7	0.36
S-27	2.52	14,345	360.6	410.1	395.1	<5	57,178	405.60	944.7	482.5
S-28	2.49	15,198	421.8	322.6	<5	<5	44,019	277.10	600.6	783.7
S-29	2.42	12,061	329.0	412.6	<5	<5	36,192	224.60	675.0	418.2
S-30	2.64	10,321	498.6	50.0	<5	<5	16,352	58.40	139.5	366.9
S-31	2.64	6548	375.3	91.2	<5	<5	17,668	112.60	138.0	599.8

Fig. 5. Extension and groundwater flow regime of the investigated perched aquifer in 2001 (TPA, 2001) (a) and 2008 (b).

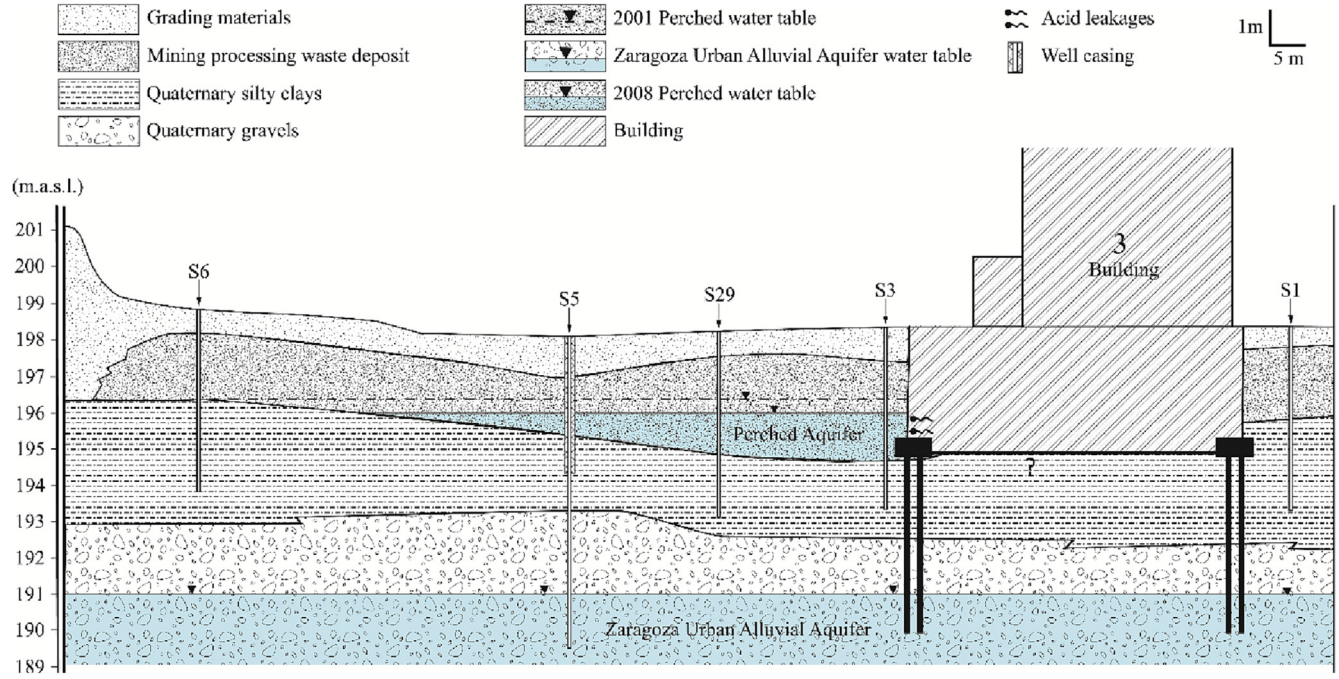

Fig. 6. Hydrogeological cross-section (A-B in Fig. 3) reflecting the situation of the perched aquifer and its relation to building 3.

In the eastern part of the perched aquifer (between buildings 2 and 3), water levels are very similar, so the flow is very low. The aquifer is bounded laterally by the buildings and by the topsoil clays in depth (Fig. 5 and Fig. 6). In the 2001 campaign, there was water overflow towards the east, evidenced by the S-18 piezometer. In contrast, in the western part of the perched aquifer, a SW-NE flow was observed, which was evident in 2001 and 2008. Moreover, the S-9 piezometer showed a downward vertical flow produced by the connection between the perched aquifer and the general alluvial aquifer, thus resulting in an intermediate water level ranging from 3.8 to 4 m deep. In addition, the perched aquifer tended to disappear further north, thus leading to the recharge of the general aquifer. This flow regime indicates that main flow paths are directed towards the southern and eastern walls of building 2 and the southern wall of building 3, thereby making the area more prone to be affected by a higher incidence of acid drainage. This higher incidence of acid drainage in the mentioned area will be contrasted by the reactive transport model, so that if it is confirmed, future mitigation procedures may consider focusing remediation preferentially, diminishing the flow towards these building walls.

There is uncertainty about the existence of water flow beneath the buildings. In principle, the excavation prior to the building's construction extracted the rubble and the industrial waste (which constituted the perched aquifer). Therefore, it is assumed that the brownfield materials were all removed and the buildings are in direct contact with fine alluvial deposits. Hence, the flow below the buildings would be inexistent.

Regarding the hydrochemistry of the perched aquifer in the sampling campaigns of 2001 (see Table 1) and 2008 (see Table 2), two main compositional groups can be distinguished. The first group consists of samples from the piezometers corresponding to the stagnation zone (S-2, S-3, S-27, S-28, S-29, S-30 y S-31). These samples are characterized by extreme acidity, with average pH values of 2.1 ± 0.24, and high concentrations of Fe (3746 ± 2759 mg/L in 2001 and 632 ± 222 mg/L in 2008) y SO_4^{2-} (14,125 ± 2790 mg/L in 2001 and 29,224 ± 16,761 mg/L in 2008), the main products from pyrite dissolution. Several of the heavy metals analysed in the water, such as Pb, Zn, Cu, As, Cd and Cr, also show very high concentrations in the stagnation zone during the maximum extension of the acid perched aquifer in 2001, reaching concentrations up to several grams per liter for Zn and Cu (e.g. 6660 mg/L of Zn in piezometer S-30), entailing high risk due to the toxicity of some of these heavy metals in case of leakage into the alluvial aquifer. The outer areas (piezometers S-4, S-8, S-10, S-18, S-19, S-21, S-22, S-26 and S-32), with respect to the stagnation zone, are characterized by higher pH values (4.6 ± 1.62) and much lower concentrations of Fe (11 ± 17 mg/L), SO_4^{2-} (3417 ± 954 mg/L) than in the previously indicated heavy metals (up to a maximum of 130 mg/L for Zn, compared to the 6660 mg/L of Zn in the stagnation area), both in the 2001 and the 2008 sampling campaigns. This compositional difference is due to the fact that water spends less time in contact with pyrite out of the stagnation zone, with lower potential for its dissolution and subsequent acidification and release of SO_4^{2-}, Fe and other heavy metals to solution. Another important outcome of this analysis is that acidification is more effective in the stagnation zone of the perched aquifer, close to the contact with the building basements, regardless the year of sampling. This means that a natural neutralization of the extreme acidity in the future is not expected, so that remediation procedures would be necessary. Further, the existence of extremely acidic groundwater (pH < 2), which is coincident with the mentioned stagnation zone, is restricted to an area of 3000 m^2 located in the southern corner between buildings 2 and 3 (Fig. 5). However, groundwater contamination by industrial waste is significant throughout the whole extension of the old chemical plant and its vicinity (debris on the river banks, filled land, etc.).

Another meaningful result is found in piezometers S-28, S-29 and S-31 (water stagnation zone), in which the molar ratio between sulfate and iron in water was very close to 2:1 in the groundwater analysed in 2001, which is consistent with the stoichiometric ratio of SO_4^{2-} and Fe in the pyrite dissolution. This demonstrates that the pyrite oxidation reactions mainly control the SO_4^{2-} and Fe concentrations in the aquifer, and that precipitation of sulfate and Fe oxi-hydroxide minerals did not significantly remove Fe and S from the solution. This is unlike what has been observed in other acid drainage examples worldwide (e.g., Hierro et al., 2014). The natural persistence of these elements in the perched aquifer should be considered when planning future mitigation procedures, as will be discussed later. Nonetheless, a different result is observed for the 2008 groundwater chemical analyses of the stagnation area, in which the molar ratios SO_4^{2-}/Fe are significantly higher than 2:1, that is, between 8:1 and 69:1. Given the lack of sulfate minerals constituting the hosting materials of the aquifer, these ratios suggest that the SO_4^{2-} was still mainly coming from pyrite dissolution and subsequent S^{2-} oxidation and increased between 2001 and 2008. Fe was probably being removed by the precipitation of Fe oxi-hydroxides, as observed in situ in several piezometers of the stagnation zone. This finding

suggests also that the pyrite dissolution increases the SO_4^{2-} concentrations with time, without any process significantly removing it out of solution. There is then the inherent risk of harmful effects of SO_4^{2-}-rich waters leading to degradation of concrete materials due to the mass formation of expansive products and the dissolution of calcium-bearing phases (Ikumi and Segura, 2019). This evolution of the SO_4^{2-} and Fe concentrations during acid drainage, as well as the precipitation of the secondary minerals will be contrasted later by the reactive transport model.

Away from the stagnation area, groundwater experienced greater flow, which reduced the interaction time with industrial waste materials, showing a slightly higher pH and much lower concentrations of Fe and SO_4^{2-}, compared to the stagnation area. In several of the piezometers, precipitation of oxi-hydroxides was observed, which has been considered as a possible process in the reactive transport model in order to understand under which conditions and in which areas these oxi-hydroxides tend to precipitate in the aquifer, favoring its cementation and enhancing water stagnation.

4.2. Reactive transport modeling of the perched urban aquifer affected by acid drainage

The previous observations and characterization were reproduced by the reactive transport model, to further understand the processes that led to the genesis of the acid drainage. It was also used as a tool to predict the long-term evolution of the aquifer, and to discuss these results in regards to planning future remediation strategies. The main hydrogeological and geochemical parameters and processes deduced by the groundwater analyses and piezometer observations are consistent with the reactive transport simulation results obtained, in terms of orders of magnitude (Fig. 7 and Fig. 8). Fig. 7 shows, at the end of the simulation (2 years), the spatial distribution of the main parameters involved in the geochemical processes modelled. Fig. 7A displays the calculated pH distribution, mainly controlled by pyrite oxidation, in the area of the perched aquifer. An important result is that pH values are much lower close to the interphase between the pyrite ash and the concrete buildings, which can be related to the fact that flow is slowed down in this area due to the much lower permeability of the concrete. This physical barrier ensures a higher residence time of the water in contact with the buildings, and a higher reaction time with pyrite, leading to a higher acidification, with pH computed values between 0.8 and 2, while in the areas further from the buildings, pH ranges from 2 to 5. This computed pH distribution is coincident with the measured values during the 2001 sampling campaign (see Table 1), coinciding with the maximum extent of the acid perched aquifer. Within the inner area of the building polygons, pH shows values up to 7.2, due to the portlandite dissolution, which consumes H+ from solution, neutralizing the acid drainage. However, this neutralization process entails a harmful impact to the concrete structure due to its partial dissolution in the building walls (Fig. 7A shows the acid groundwater infiltrating through approximately 3–5 m inside the building walls). The pyrite dissolution is displayed in terms of dissolution rate (Fig. 7B) and remaining moles (Fig. 7C) at the end of the simulation, with respect to the initial available amount of 1.65 mol/kgw. In both cases, the most remarkable result is that pyrite dissolution has a maximum incidence of up to $5.15 \cdot 10^{-4}$ mol/kgw/day in the areas close to the building walls, which is consistent with the fact that the interaction time between the groundwater and pyrite is higher in this stagnation area than in the borders of the aquifer. Nevertheless, the remaining amounts of pyrite after the two-year simulation are between 1.65 and 1.35 mol/kgw; between 0 % and 18 % of the initial pyrite has been dissolved, depending on the proximity to the stagnation area. These results indicate that the availability of pyrite is not a limiting factor for the development of extreme acidity in the hanging aquifer, as these conditions are achieved by dissolving only a small proportion of the total available residual pyrite. Thus, the main factor controlling this acidification in the system is the flow regime and the subsequent contact time of water with pyrite, whereas acidification is significantly greater in the stagnation area regardless of the amount of available pyrite. The implications of these findings for the planning of future mitigation measures will be discussed subsequently.

The main reaction products of the pyrite oxidation, Fe^{2+} and S^{2-}, are rapidly oxidized during the simulation to Fe^{3+} and SO_4^{2-}, so that the concentrations of the reduced species of Fe and S are negligible and not worth displaying. A similar spatial pattern to that of the pyrite dissolution can be observed for the total Fe (Fig. 7D) and SO_4 (Fig. 7E) concentrations. Close to the interphase between the pyrite ash and the concrete walls, they reach maximum values of up to 10,000 mg/L and 34,000 mg/kgw, respectively, with a higher pyrite dissolution and the subsequent higher Fe and SO_4 released to the solution. In areas further away from the buildings, Fe and SO_4 concentrations range in several orders of magnitude lower than near them, finding values close to the initial solution of the irrigation water. It is also remarkable that, as in the case of the computed pH vs. measured pH, both computed pH, Fe and SO_4 concentrations are close to the values measured in the groundwater analyses, or at least in the same magnitude order. Thereby, it can be stated that the reactive transport model has reproduced the measured final chemistry of the perched aquifer in terms of the main parameters involved in the ongoing chemical reactions. This reproduction now provides a precise tool for predicting the future evolution of the modelled chemical reactions and parameters, which is necessary in planning future remediation procedures. This represents one of the main objectives of this paper.

Another important outcome of the reactive transport model results relates to the precipitation of secondary minerals; pH, Fe and SO_4 contents released by the pyrite dissolution control the S.I. and precipitation of the secondary minerals considered – ferrihydrite (Fig. 7F) and jarosite-K (Fig. 7G). The S.I. of both phases is mainly controlled by pH, Fe (III) and SO_4 concentrations, the latter only affecting jarosite SI. Ferrihydrite stability is typically found at pH > 4.8, while jarosite-K is stable and can precipitate in a pH range of 2–4 (Keene et al., 2010). Thus, ferrihydrite only reaches oversaturation and precipitation close to the building walls, where the pH neutralization leads to the pH > 4.8 needed for its precipitation. Jarosite-K precipitates in the external areas, further away from the stagnation area, where the pH values are over 2.5, mainly related to the areas where the Fe (III) oxidation mechanism for pyrite dissolution has not started. The model shows that the dominance of this oxidation mechanism, along with the subsequent extreme acidity (pH < 2), propagates during the simulation time from the stagnation area towards the aquifer's outer limits. The importance of this computed distribution is that, instead of expecting future natural attenuation of the acid drainage, the model shows that the extreme acidity front would tend to propagate across a higher area, potentially affecting new buildings. Propagation of the secondary minerals precipitation front can be responsible for cementation in the base of the pyrite ash in this area, thereby enhancing water stagnation, with a positive feedback effect on pyrite oxidation and water acidification. The implications of this propagation process for remediation actions will be discussed later.

Another important result of the reactive transport model is the calculation of the effect of portlandite dissolution (Fig. 7H) on Ca concentrations (Fig. 7I) and gypsum S.I. (Fig. 7J). The maximum portlandite dissolution rates, up to $1.87 \cdot 10^{-5}$ mol/kgw/day, are reached in the interphase pyrite ash – concrete, especially in the areas of lower pH values (**see** Fig. 7A). The portlandite dissolution is pH neutralizing and locally releases, in the interphase area, an important amount of Ca to solution, reaching maximum values of 436 mg/L. This, together with the maximum concentrations of SO_4, entails a local increase in the gypsum SI in the eastern wall of building 2. This is the only area where gypsum almost reaches oversaturation, and thereby potential precipitation, if slightly higher simulation times are considered. This SO_4^{2-}-rich water interaction with concrete could drastically enhance its alteration in the future (e.g., Ikumi and Segura, 2019).

The temporal evolution of the main hydrochemical variables along a streamline in the perched aquifer (see Fig. 4**:** P1, P2, P3 and P4) is shown in Fig. 8. In this figure, only processes related to the acid drainage are shown, since the processes and parameters related to portlandite dissolution are restricted to a reduced area in the model and do not show a significant temporal variability or effect over water chemistry. The simulation results show that pH (Fig. 8A) decreases over time at all the selected points

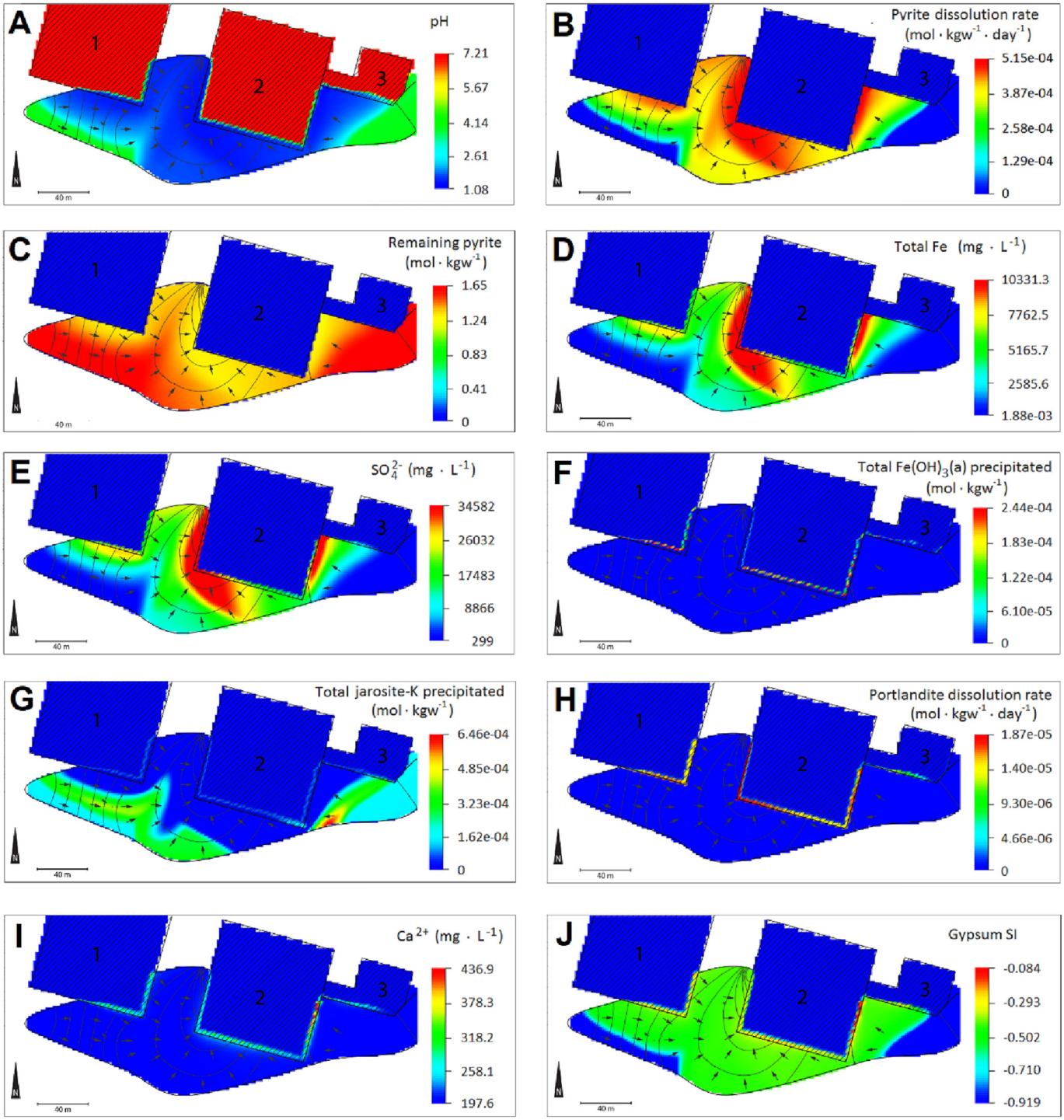

Fig. 7. Spatial distribution of (A) pH (B) pyrite dissolution rate (C) remaining pyrite moles (D) total Fe concentration (E) sulfate concentration (F) ferrihydrite precipitated moles (G) jarosite-K precipitated moles (H) portlandite dissolved moles (I) Ca concentration (J) gypsum SI, calculated with the 2-year PHAST reactive transport model.

along the streamline, mainly controlled by pyrite oxidation (Fig. 8B), so that the minimum pH values (ranging from 1 to 1.5), are reached in the stagnation area (P4), where the pyrite dissolved mass is at its maximum due to higher water residence time. It is also worth highlighting that pH decreases with an approximately constant rate, excepting a strong decrease rate below 3.5 related to Fe (III) oxidation of pyrite triggered approximately below this pH value. Since this mechanism shows a faster kinetic dissolution rate compared to O_2 oxidation, acidification is rapidly enhanced once Fe (III) starts oxidizing pyrite. This is observed at different times for each point, since the water residence time for pyrite dissolution is at its maximum at P4 and at a minimum at P1, where a fast pH drop below 3.5 is observed after 600 days. In the stagnation area (P4) and the close points (P2 and P3), the drastic pH drop below 3.5 starts after 300 days. This is consistent with propagation of the Fe (III) oxidation mechanism front towards the outer areas, with respect to the stagnation zone near buildings 2 and 3, which is displayed in Fig. 7. The computed time distribution of this propagation provides a propagation rate of this extreme acidity front (pH < 2) of approximately 30 m/year under the constant flow regime considered in the model.

Both pyrite oxidation mechanisms (O_2 and Fe (III) oxidation) entail the release of Fe (II) to solution, which is rapidly oxidized to Fe (III). The Fe

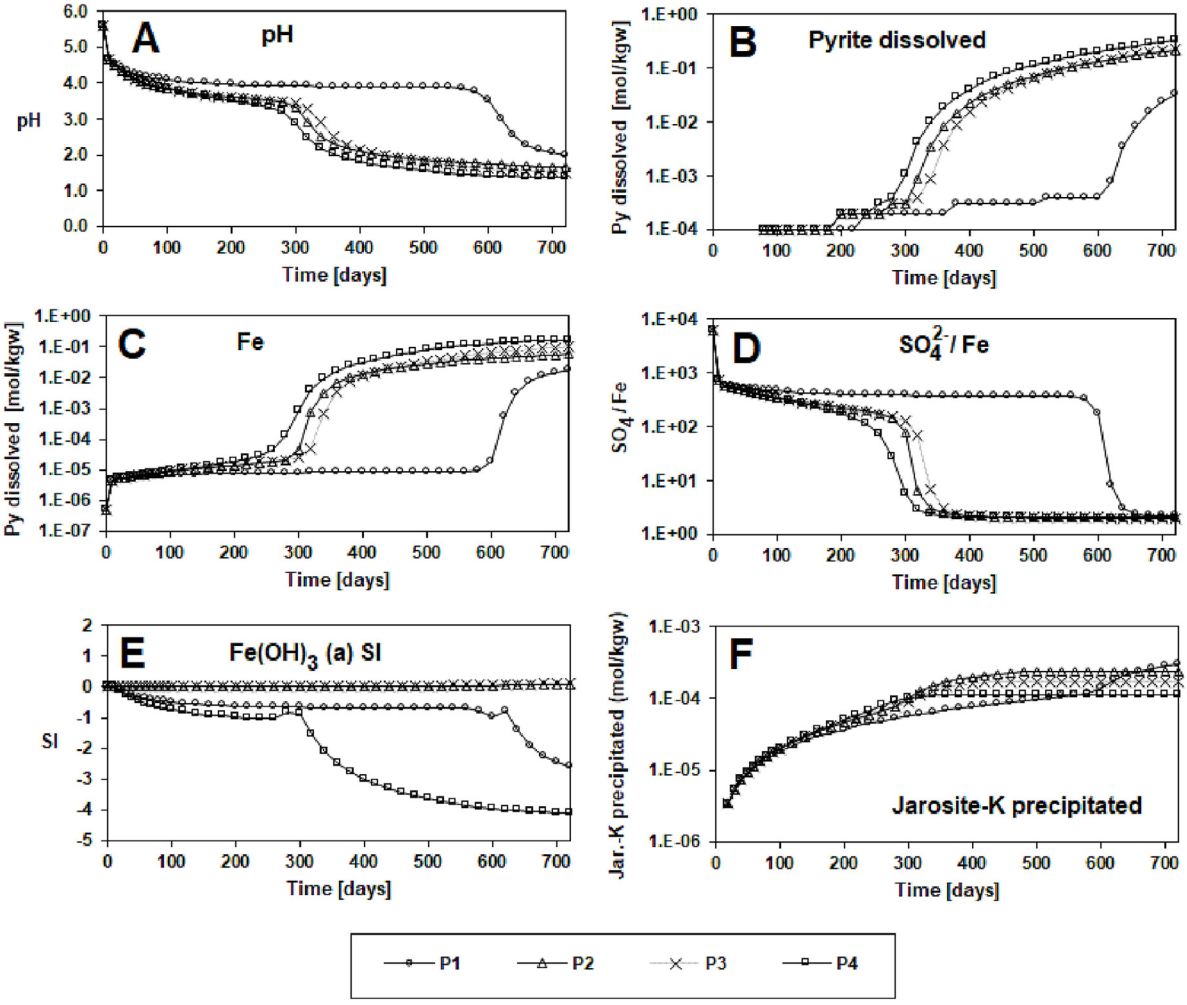

Fig. 8. Temporal evolution of (A) pH (B) pyrite dissolved moles (C) total Fe concentration (D) SO_4/Fe ratio (E) ferrihydrite SI (F) jarosite-K precipitated moles. The vertical axes are displayed in logarithmic scale (log 10).

oxidation rate is higher at the points and time coincident with the highest pyrite mass dissolution values, as it increases the oxidizing character of the aquifer. This entails higher values of total dissolved Fe (Fig. 8C), and Fe (III) dominating over Fe (II), since the pyrite dissolution starts at the beginning of the simulation. Fe (III) concentration is several orders of magnitude higher than Fe (II), due to the oxidizing environment maintained with the constant O_2 re-equilibrium in solution up to the atmospheric partial pressure. The maximum values of dissolved Fe, up to 0.17 mol/kgw (9490 mg/L), are reached by the end of the simulation, related to the higher pyrite dissolved mass, and these values increase in the streamline from P1 to the stagnation area in P4. The computed ratio SO_4^{2-} – Fe (Fig. 8D) was maintained, indicating that the effect of the precipitation rate of the secondary minerals over sulfate and Fe contents is negligible compared to the dissolution rate of pyrite; otherwise the SO_4-Fe ratio would deviate from the 2:1 trend. This is consistent with the measured values, which also fit the 2:1 ratio in the stagnation zone, except for the 2008 measurements, which show higher SO_4^{2-}/Fe ratio. This is probably due to the precipitation of slightly higher amounts of Fe oxi-hydroxides than predicted by the model, which provides closer ratios to those measured if simulation time is increased.

In line with the distribution of pyrite oxidation and secondary minerals precipitation, the most favorable pH conditions for ferrihydrite precipitation (pH > 4.8) are reached by the end of the simulation in P2 and P3, where the ferrihydrite SI (Fig. 8E) is closer to 0 in the area with high Fe (III) concentrations but further from the minimum pH of the stagnation area. However, as previously shown in Fig. 7F, ferrihydrite only precipitates induced by the pH neutralization produced by portlandite dissolution that takes place locally in the walls of the buildings. Jarosite-K widely precipitates over time and along the streamline, so that the jarosite precipitated mass (Fig. 8F) is displayed instead of the SI. The precipitation of this phase increases over the simulation time at all points, reaching low precipitated amounts up to 3E-04 mol/kgw, much lower than the pyrite dissolved mass. Jarosite-K precipitation stops after the pH values are approximately below 2, which is out of the theoretical stability pH range for this mineral. Interestingly, neither ferrihydrite nor jarosite-K precipitation have a significant effect on the groundwater chemistry, but they could contribute to the aquifer cementation, favoring water stagnation close to the building walls.

Precipitation of ferrihydrite has also been observed in piezometers. Several authors (Blowes et al., 1991; Boorman, 1976) identified that the cementation of tailings was caused by Fe(III) minerals. This cementation generates an impermeable barrier called *hardpan layers*. Thus, this precipitation process could have been crucial in sealing the base of the industrial waste, therefore contributing to and enhancing both the generation of the perched aquifer and the acidification of the groundwater due to the increase of water residence times.

4.3. Remediation and envrionmental management outcomes

After characterization of the acid perched aquifer and the water sample analyses, the observations in piezometers and the simulation results show that the ongoing acid drainage represents an environmental problem that

needs to be properly remediated in the next years, given the temporal and spatial evolution of the acidity reproduced by the reactive transport model. Considering that the simulation indicates only a small fraction of the total pyrite mass is dissolved, and the ultra-acidic front is migrating towards the external borders of the aquifer, this means that the acid drainage would continue and could show an even higher intensity in the future. Thus, remediation procedures are essential to reduce the extension of the perched aquifer and the interaction of the acid drainage with the concrete basements of the buildings as much as possible.

A possible final solution for this environmental problem could be the complete removal of waste from the affected area – about 10,000 m^3 between buildings 2 and 3 (Fig. 5). However, because the residue occupied far more extension than just the problem area, the construction company dismissed that solution due to limited economic resources. Instead of removing the materials, the company decided to extract the contaminated water with pumps through the existing piezometers. Pumping of the acidic groundwater of the perched aquifer began in February 2008, using a compressed-air-powered double-diaphragm pump. The results were unexpected and unsuccessful: 12 h of pumping at the S-27 piezometer removed only 8000 L. After 15 h of simultaneously pumping at piezometers S-2, S-28 and S-20, 12,000 l were removed. After the last 15 h of pumping, the water level dropped to the base of the piezometers, while the observation piezometers recorded subtle water level decreases. The hydraulic characteristics observed are, therefore, markedly different from those reported in 2001 (TPA, 2001). The construction company proposed to drill a large-diameter well to pump out the water, but this alternative was not accepted by the Local Water Authority due to the high risk of connecting the contaminated perched aquifer with the regional alluvial aquifer. Finally, it was decided to build a retaining wall beside the garage of building 3, thus avoiding contact with the acidic water. Additionally, the acidic groundwater of the aquifer is periodically pumped.

This collector system has effectively reduced the extent of the perched aquifer, with the aquifer disappearing in seven piezometers, indicating the success of the rainwater trap. However, the collector has not significantly altered the chemical composition or extreme acidity conditions that still affect the buildings in the remaining area of the perched aquifer. Hence, additional remediation actions will be necessary in the future. The modeling results also demonstrate that extreme acidity is achieved by dissolving only a small proportion of the available pyrite. This finding implies that the primary limiting factor in this process is the contact time of water with the pyrite, regardless of the amount of sulfide available. Therefore, if pyrite waste removal is considered, complete removal of all waste material rather than partial removal would be necessary. Actions aimed at reducing the main limiting factor, such as flow control and reducing water residence time in contact with pyrite waste (e.g., periodic water pumping or additional water collectors to prevent infiltration), would be more efficient than partial pyrite waste removal. Considering that the majority of recharge is attributed to artificial irrigation as opposed to rainfall, and since the numerical model results demonstrate that the flow and reaction time between water and pyrite roasting residues is the primary limiting factor for extreme acidification, it is strongly recommended to significantly reduce artificial irrigation in the green areas surrounding the Almozara aquifer.

Regarding validation of the numerical model, the hydrogeological and geochemical parameters and processes deduced from groundwater analyses and piezometer observations align with the reactive transport simulation results in terms of magnitude. This indicates that the model provides a precise tool for predicting the future evolution of the modelled chemical reactions and parameters. In the water stagnation zone, the proximity in the ratio between sulfate and iron in water of 2:1 indicates that the pyrite oxidation reactions mainly reactions controlling the SO_4^{2-} and Fe concentrations in the aquifer, and that precipitation of secondary minerals was not significantly removing Fe and S out of solution by 2001, necessitating a high persistence of these elements in the water. On the contrary, samples from 2008 show higher sulfate – iron ratios, indicating Fe removal out of solution by ferrihydrite precipitation, although sulfate values still increase and residual pyrite remains. This implies that, when planning for mitigation, natural attenuation of the increased concentrations of SO_4^{2-} cannot be expected. This poses a risk to the quality of groundwater in case of leaks from the perched aquifer to the alluvial aquifer, and also due to the potential degradation of concrete by the sulfate-rich solutions. Therefore, additional remediation measures are necessary in addition to preventive measures.

The model shows that the dominance of this oxidation mechanism, along with the subsequent extreme acidity (pH < 2), propagates during the simulation time from the stagnation area towards the aquifer's outer limits. The computed time for this propagation provides a propagation rate of this extreme acidity front of approximately 30 m/year under the flow regime considered in the numerical model. This calculated propagation rate suggests that it would be advisable to monitor the lateral spread of the extreme acidity front through periodic pH measurement campaigns performed at least once a year. Further, mitigation efforts should focus on this limit to prevent its further propagation. In particular, the use of surface water collectors placed between the water recharge sources and the extreme acidity front could help reduce the flow rate and diminish the propagation rate. Additionally, the precipitation front of jarosite-K is advancing towards the outer areas, away from the stagnation zone, so that cementation of the aquifer due to this process could promote water stagnation and pyrite dissolution. Further research is needed to investigate the correlation between secondary mineral precipitation in acid drainage and the subsequent local permeability reduction, enhancing water stagnation, pyrite oxidation, and water acidification.

Finally, regarding the acidic water interaction with the concrete materials in the inner area of the building polygons, the interaction of acidic water with concrete materials has been computed. The pH values reach up to 7.2 as a result of portlandite dissolution, effectively neutralizing the acid drainage. This contrasts highly with the pH values below 2 a few meters out of the concrete polygon. However, it is important to note that this neutralization process has a detrimental impact on the concrete structure due to partial dissolution occurring in the building walls (see Fig. 7A). Thus, in addition to the suggested prevention and remediation procedures, it would be recommended in the future to monitor the effects of acid drainage on the concrete in the southern walls of the buildings, through petrographic microscope analysis, for instance.

5. Conclusions

The hydrogeology and geochemistry of an urban area built over a former industrial zone and presenting acid drainage problems in underground car parks was examined. A reactive transport model has been developed for acid drainage from pyrite roasting waste in an urban area, where flow is controlled by artificial physical barriers represented by building basements, resulting in significant differences in water residence time across different zones of the model. Drilling and piezometer construction, along with groundwater samples, revealed the existence of a perched aquifer within old sulphide mill tailings. A detailed hydrogeological and hydrochemical characterization was carried out, which served as the basis for the development of a groundwater flow reactive transport model. The chemical analysis of the groundwater sampled from the perched aquifer provided extreme acidity values (pH < 2), high SO_4 (up to 57,000 mg/L) and Fe (up to 7250 mg/L) contents and high concentrations of several heavy metal trace elements such as Pb, Zn, Cu, As, Cd and Cr, reaching values of several grams per liter. The characterization of the aquifer, water sample analyses, observations in piezometers, and reactive transport modeling, have exposed the urgent need for proper remediation of the ongoing acid drainage, due to a propagating front of extreme acidity (pH < 2) computed as approximately 30 m/year (under constant recharge assumption used in the reactive transport model) and due to the remaining sulfide available in the pyrite waste deposits. The model predicted that only a maximum of 18 % of the initially available pyrite has been dissolved. This suggests that the acid drainage will continue and potentially intensify in the future. Therefore, remediation procedures are essential to minimize the extent of the perched aquifer and mitigate the interaction of acid drainage with concrete structures.

The measured groundwater chemistry has been successfully reproduced by the reactive transport model, validating its predictive potential. The simulation results indicate that the extreme acid character of the groundwater (pH < 2) is drastically triggered by kinetically controlled Fe^{+3} oxidation for pyrite, tends to propagate towards the outer limits of the perched aquifer. It is limited by the water residence time in contact with the mineral, rather than by the initial sulfide availability Therefore, reduction of artificial irrigation in the area surrounding the Almozara aquifer is recommended.

To address this environmental problem, a possible solution is the complete removal of waste material from the affected area. However, economic constraints limited the feasibility of this approach in this study area. Instead, the extraction of contaminated water through pumps installed in piezometers was attempted. However, the results were unexpected and unsuccessful due to the low volumes extracted, indicating the need for alternative remediation strategies. The construction of a water collector alongside the garage of one of the buildings in 2005 proved to be an effective measure to significantly reduce the extent of the perched aquifer; however, the extremely acidic water in contact with the southern walls of buildings 2 and 3 was not solved in the remaining areas of the perched aquifer, mainly in the water stagnation zone. Therefore, additional remediation actions will be necessary in the future. In particular, monitoring the lateral spread of the extreme acidity front through periodic pH measurements is crucial for effective mitigation. Implementing surface water collectors between water recharge sources and the extreme acidity front can help reduce the flow rate and slow down the propagation.

The advancement of the jarosite-K precipitation front away from the stagnation zone suggests that cementation of the aquifer could further enhance water stagnation and pyrite dissolution. Further research into the correlation between secondary mineral precipitation and local permeability reduction would be needed to address this effect when designing the reactive transport models. For instance, coupling the permeability change to each iteration of the model could help in increasing the precision of the flow regime reproduction, more important in cases like the scenario that has been studied in this paper, where water flow represents the main limiting factor of extreme water acidity development.

Finally, the interaction of acidic water with concrete materials in the inner area of the building polygons has been shown to have both pH neutralizing and harmful effects. While portlandite dissolution locally neutralizes acid drainage, it also leads to partial dissolution of concrete in building walls. Therefore, in addition to preventive and remediation measures, monitoring the effects of acid drainage on concrete structures, particularly in southern walls, is recommended.

The numerical model successfully reconstructed the geochemical evolution and the flow regime leading to the formation of a stagnation zone in a hanging aquifer, where water acidification increases significantly to pH < 2 due to pyrite oxidation by Fe (III) under conditions of prolonged reaction time. The model predicts the propagation of an extreme acidity front beyond the stagnation zone, indicating that, in cases where acidification is limited by flow in acid drainage issues, the installation of water collectors between the recharge area and the acidification front may be the most efficient remediation technique, together with artificial recharge restriction and water pump out being performed periodically. These findings aim to serve as a background in the numerical modeling of acid drainage in urban areas.

The findings of this study have broader implications for the study and mitigation of acid drainage effects in urban areas worldwide. The temporal and spatial evolution of acidity, the potential future intensification of acid drainage, and the detrimental effects on aquifers and concrete structures are common challenges faced in urban environments globally. The remediation strategies proposed in this study (complete waste removal, retaining walls, periodic pumping, and surface water collectors as the most successful procedures in this scenario) can serve as valuable references for other locations grappling with similar acid drainage issues.

Future research on the reactive surface areas and mineral composition of these pyrite ash deposits needs to be addressed, considering the high sensitivity of reactive transport models to these parameters, representing one of the main model limitations in this study. Nevertheless, the results of this paper through the validation of a reactive transport model with the groundwater chemical analysis has been used to guide the planning of future remediation actions to mitigate the acid drainage process. Thus, these outcomes are expected to serve as a practical background for the assessment of acid drainage in urban aquifers globally, since urbanization on former industrial land occurs in most cities worldwide.

Data availability

Data will be made available on request.

Declaration of competing interest

The authors declare that they have no known competing financial interests or personal relationships that could have appeared to influence the work reported in this paper.

Acknowledgements

This research was partially supported by the SAGE4CAN project, which is funded by the Spanish Research Agency (AEI project PID2020-114218RA-100).

CRediT authorship contribution statement

Conceptualization, J.A.S. and A.G.G.; methodology, hydrogeochemical sampling by J.A.S. and reactive transport modeling by J.J.B and A.G.G.; formal analysis, J.C.S.; investigation, M.A.M.; resources, J.M.L.; data curation, C.B.; writing—original draft preparation, J.J.B and A.G.G.; writing—review and editing, M.A.M. and N.C.P.; visualization, J.M.L. and C.B.; supervision, A.G.G.; All authors have read and agreed to the published version of the manuscript.

References

Alcaraz, M., García-Gil, A., Vázquez-Suñé, E., Velasco, V., 2016. Advection and dispersion heat transport mechanisms in the quantification of shallow geothermal resources and associated environmental impacts. Sci. Total Environ. 543, Part A, 536–546.

Allen, A., Da Silva, N.L.A., Corubolo, E., 1999. Environmental Problems and Opportunities of the Peri-urban Interface and their Impact upon the Poor. Peri-urban Interface Project. Development Planning Unit, University College London, Strategic Environmental Planning and Management for the Peri-urban Interface, p. 43.

Ana, P., 2018. Status of Local Soil Contamination in Europe - Revision of the Indicator. European Union Agency for Asylum, Malta Retrieved from https://policycommons.net/artifacts/3373102/status-of-local-soil-contamination-in-europe/4171906/ on 05 Jul 2023. CID: 20.500.12592/4rzrw2.

Anawar, H.M., 2015. Sustainable rehabilitation of mining waste and acid mine drainage using geochemistry, mine type, mineralogy, texture, ore extraction and climate knowledge. J. Environ. Manag. 158, 111–121.

Appleyard, S.J., Angeloni, J., Watkins, R., 2006. Arsenic-rich groundwater in an urban area experiencing drought and increasing population density, Perth, Australia. Appl. Geochem. 21 (1), 83–97.

Ayora, C., Macías, F., Torres, E., Lozano, A., Carrero, S., Nieto, J.M., ... Castillo-Michel, H., 2016. Recovery of rare earth elements and yttrium from passive-remediation systems of acid mine drainage. Environ. Sci. Technol. 50 (15), 8255–8262.

Bambra, C., Robertson, S., Kasim, A., Smith, J., Cairns-Nagi, J.M., Copeland, A., et al., 2014. Healthy land? An examination of the area-level association between brownfield land and morbidity and mortality in England. Environ. Plan. A Econ. Space 46, 433–454.

Bech, J., 2020. Soil contamination and human health: part 1—preface. Environ. Geochem. Health 42.

Bell, L.C., Ward, S.C., Kabav, E.D., Jones, C.J., 1989. Mine tailings reclamation in australia - an overview. Proceedings of the Conference - Reclamation, a Global Perspective. Vols 1 and 2, pp. 769–781.

Berg, W., Barrau, E., Rhodes, L., 1975. Plant growth on acid molybdenum mill tailings as influenced by liming, leaching and fertility treatments. Symposium of the British Ecological Society.

Blowes, D.W., Reardon, E.J., Jambor, J.L., Cherry, J.A., 1991. The formation and potential importance of cemented layers in inactive sulfide mine tailings. Geochim. Cosmochim. Acta 55, 965–978.

Boorman, R., 1976. Chemical processes in abandoned sulfide tailings dumps and environmental implications for northeastern New Brunswick. Can. Inst. Mining Metall. Bull. 69, 86–96.

Charlton, S.R., Parkhurst, D.L., 2011. Modules based on the geochemical model PHREEQC for use in scripting and programming languages. Comput. Geosci. 37, 1653–1663.

Chen, M., Ye, C., 2014. Differences in pattern and driving forces between urban and rural settlements in the coastal region of Ningbo, China. Sustainability 6, 1848–1867.
Chen, L., Ren, C., Zhang, B., Wang, Z., Liu, M., 2018. Quantifying urban land sprawl and its driving forces in Northeast China from 1990 to 2015. Sustainability 10, 188.
Chen, G., Ye, Y., Yao, N., Hu, N., Zhang, J., Huang, Y., 2021. A critical review of prevention, treatment, reuse, and resource recovery from acid mine drainage. J. Clean. Prod. 329, 129666.
Dean, S.A., 1982. Acid Drainage from Abandoned Metal Mines in the Patagonia Mountains of Southern Arizona.
Del Giudice, V., De Paola, P., Bevilacqua, P., Pino, A., Del Giudice, F.P., 2020. Abandoned industrial areas with critical environmental pollution: evaluation model and stigma effect. Sustainability 12.
Domènech, C., Canals, À., Soler, A., Sabanès, A., Dumestre, A., 2017. Evolution assessment of soils contaminated by roasted pyrite wastes. Proc. Earth Planet. Sci. 17, 432–435.
Egiebor, N.O., Oni, B., 2007. Acid rock drainage formation and treatment: a review. Asia Pac. J. Chem. Eng. 2, 47–62.
Elliott, P., Ragusa, S., Catcheside, D., 1998. Growth of sulfate-reducing bacteria under acidic conditions in an upflow anaerobic bioreactor as a treatment system for acid mine drainage. Water Res. 32, 3724–3730.
Eurostat., 2016. Urban Europe – Statistics on Cities, Towns and Suburbs. Eurostat, Luxembourg.
Fuller, W.H., Lanspa, K., 1975. Uptake of Iron and Copper by Sorghum From Mine Tailings. Wiley Online Library.
Gabarrón, M., Babur, O., Soriano-Disla, J.M., Faz, A., Acosta, J.A., 2018. Composition and risk assessment of roasted pyrite ash from fertiliser production. Chemosphere 209, 277–285.
Garcia-Gil, A., Vazquez-Sune, E., Schneider, E.G., Sanchez-Navarro, J.A., Mateo-Lazaro, J., 2014. The thermal consequences of river-level variations in an urban groundwater body highly affected by groundwater heat pumps. Sci. Total Environ. 485-486, 575–587.
García-Gil, A., Vázquez-Suñé, E., Sánchez-Navarro, J.Á., Mateo Lázaro, J., Alcaraz, M., 2015. The propagation of complex flood-induced head wavefronts through a heterogeneous alluvial aquifer and its applicability in groundwater flood risk management. J. Hydrol. 527, 402–419.
García-Gil, A., Mejías Moreno, M., Garrido Schneider, E., Marazuela, M.Á., Abesser, C., Mateo Lázaro, J., et al., 2020. Nested shallow geothermal systems. Sustainability 12, 5152.
Grundl, T., Delwiche, J., 1993. Kinetics of ferric oxyhydroxide precipitation. J. Contam. Hydrol. 14 (1), 71–87.
Guillén, M.T., Delgado, J., Albanese, S., Nieto, J.M., Lima, A., De Vivo, B., 2011. Environmental geochemical mapping of Huelva municipality soils (SW Spain) as a tool to determine background and baseline values. J. Geochem. Explor. 109, 59–69.
Hierro, A., Olías, M., Ketterer, M.E., Vaca, F., Borrego, J., Cánovas, C.R., Bolivar, J.P., 2014. Geochemical behavior of metals and metalloids in an estuary affected by acid mine drainage (AMD). Environ. Sci. Pollut. Res. 21, 2611–2627.
Hiji, M.F., Ntalikwa, J.W., Vuai, S.A., 2014. Producing sulphuric acid in Tanzania and potential sources: a review. Am. J. Chem. Appl. 1, 40–44.
Hossner, L.R., Hons, F.M., 1992. Reclamation of mine tailings. In: Lal, R., Stewart, B.A. (Eds.), Soil Restoration: Soil Restoration. 17. Springer, New York, New York, NY, pp. 311–350.
Huminicki, D.M., Rimstidt, J.D., 2009. Iron oxyhydroxide coating of pyrite for acid mine drainage control. Appl. Geochem. 24 (9), 1626–1634.
Ikumi, T., Segura, I., 2019. Numerical assessment of external sulfate attack in concrete structures. A review. Cem. Concr. Res. 121, 91–105.
Jarah, S.H., Zhou, B., Abdullah, R.J., Lu, Y., Yu, W., 2019. Urbanization and urban sprawl issues in city structure: a case of the Sulaymaniah Iraqi Kurdistan region. Sustainability. 11.
Julián, P.L.L., Anchuela, P., Gimeno, C.R., Lázaro, B.B., Cordero, J.R., Ballester, P.C., Pocoví, J.A., Sánchez, J., Mihi, E., Jiménez, G., 2020. Evaluación de la movilidad potencial de metales en escorias industriales presentes en el subsuelo de un entorno urbano (barrio de la Almozara, Zaragoza). Geogaceta 68, 39–42.
Keene, A., Johnston, S., Bush, R., Sullivan, L., Burton, E., 2010, August. Reductive dissolution of natural jarosite in a tidally inundated acid sulfate soil: geochemical implications. 19th World Congress of Soil Science, Soil Solutions for a Changing World, pp. 1–6.
Kefeni, K.K., Msagati, T.A., Mamba, B.B., 2017. Acid mine drainage: prevention, treatment options, and resource recovery: a review. J. Clean. Prod. 151, 475–493.
Kong, S., Lu, B., Ji, Y., Zhao, X., Chen, L., Li, Z., et al., 2011. Levels, risk assessment and sources of PM10 fraction heavy metals in four types dust from a coal-based city. Microchem. J. 98, 280–290.
Li, X., Liu, L., Wang, Y., Luo, G., Chen, X., Yang, X., et al., 2013. Heavy metal contamination of urban soil in an old industrial city (Shenyang) in Northeast China. Geoderma 192, 50–58.
Lichtner, P.C., 1996. Continuum formulation of multicomponent-multiphase reactive transport. Rev. Mineral. 34, 1–82.
Lin, Z., Quvarfort, U., 1996. Predicting the mobility of Zn, Fe, Cu, Pb, Cd from roasted sulfide (pyrite) residues—a case study of wastes from the sulfuric acid industry in Sweden. Waste Manag. 16, 671–681.
Malmström, M.E., Berglund, S., Jarsjö, J., 2008. Combined effects of spatially variable flow and mineralogy on the attenuation of acid mine drainage in groundwater. Appl. Geochem. 23 (6), 1419–1436.
Meuser, H., 2010. Contaminated Urban Soils. vol. 18. Springer Science & Business Media.
Naidu, G., Ryu, S., Thiruvenkatachari, R., Choi, Y., Jeong, S., Vigneswaran, S., 2019. A critical review on remediation, reuse, and resource recovery from acid mine drainage. Environ. Pollut. 247, 1110–1124.
Nordstrom, D.K., 2000. Advances in the hydrogeochemistry and microbiology of acid mine waters. Int. Geol. Rev. 42, 499–515.
Oliveira, M.L., Ward, C.R., Izquierdo, M., Sampaio, C.H., de Brum, I.A., Kautzmann, R.M., et al., 2012. Chemical composition and minerals in pyrite ash of an abandoned sulphuric acid production plant. Sci. Total Environ. 430, 34–47.
Parkhurst, D.L., Appelo, C.A.J., 2013. Description of input and examples for PHREEQC version 3. A computer program for speciation, batch reaction, one dimensional transport, and inverse geochemical calculations. Techniques and methods (U.S. Geological Survey, Ed.), Book 6, Chap. A43. U.S.
Parkhurst, D.L., Kipp, K.L., Engesgaard, P., Charlton SRJUGst, methods, 2004. PHAST—A Program for Simulating Ground-water Flow, Solute Transport, and Multicomponent Geochemical Reactions. 6 p. A8.
Pérez-López, R., Nieto, J.M., de Almodóvar, G.R., 2007. Immobilization of toxic elements in mine residues derived from mining activities in the Iberian Pyrite Belt (SW Spain): laboratory experiments. Appl. Geochem. 22, 1919–1935.
Runkel, M., Sturm, P., 2009. Pyrite roasting, an alternative to sulphur burning. J. South. Afr. Inst. Min. Metall. 109, 491–496.
Solcova, O., Krystynik, P., Dytrych, P., Bumba, J., Kastanek, F., 2022. Typical groundwater contamination in the vicinity of industrial brownfields and basic methods of their treatment. Ecotoxicol. Environ. Saf. 233, 113325.
Song, B., Zeng, Z., Almatrafi, E., Shen, M., Xiong, W., Zhou, C., Wang, W., Zeng, G., Gong, J., 2022. Pyrite-mediated advanced oxidation processes: applications, mechanisms, and enhancing strategies. Water Res. 118048.
Sorensen, D.L., Kneib, W.A., Porcella, D.B., Richardson, B.Z., 1980. Determining the Lime Requirement for the Blackbird Mine Spoil. Wiley Online Library.
Soriano-Disla, J.M., Spille, U., Gabarrón, M., Faz, Á., Acosta, J.A., 2018. Evaluation of strategies for mitigating risks associated with metals in pyrite ash. J. Environ. Manag. 217, 403–410.
Tomiyama, S., Igarashi, T., 2022. The potential threat of mine drainage to groundwater resources. Curr. Opin. Environ. Sci. Health 100347.
TPA, 2001. Investigación detallada del subsuelo para el diagnóstico medioambiental del barrio de La Química (Zaragoza). Zaragoza City Council, Madrid.
Vasilache, N., Diacu, E., Modrogan, C., Chiriac, F.L., Paun, I.C., Tenea, A.G., et al., 2022. Groundwater quality affected by the pyrite ash waste and fertilizers in Valea Calugareasca. Romania. 14, 2022.
Williamson, M.A., Rimstidt, J.D., 1994. The kinetics and electrochemical rate-determining step of aqueous pyrite oxidation. Geochim. Cosmochim. Acta 58, 5443–5454.
Wong, C.S.C., Li, X., Thornton, I., 2006. Urban environmental geochemistry of trace metals. Environ. Pollut. 142, 1–16.

Web references

CHE: regional groundwater analysis monitoring network in the Ebro alluvial aquifer. Last Consulted in April 2023: http://www.datossubterraneas.chebro.es:81/WCAS/